

The optical variability of Supermassive Black Hole Binary Candidate PG1302-102:

Periodicity and perturbation in the light curve

ANDJELKA B. KOVAČEVIĆ,¹ LUKA Č. POPOVIĆ,^{2,1} SAŠA SIMIĆ,³ AND DRAGANA ILIĆ¹

¹*Department of astronomy, Faculty of mathematics, University of Belgrade*

Studentski trg 16, Belgrade, 11000, Serbia

²*Astronomical observatory Belgrade*

Volgina 7, P.O.Box 74 11060, Belgrade, 11060, Serbia

³*Faculty of Sciences, Department of Physics, Univerisity of Kragujevac*

Radoja Domanovica 12, Kragujevac, 34000, Serbia

(Received; Revised; Accepted)

ABSTRACT

The photometric light curve of PG1302-102 shows periodic variability which makes this object one of the most plausible supermassive black hole binary candidate. Interestingly, the most recent study of its updated optical light curve reports a decrease in a significance of periodicity which may suggest that the binary model is less favorable. Here, we model the PG 1302-102 light curve, spanning almost 20 years, with a supermassive black hole binary system in which a perturbation in the accretion disk of more massive component is present. Our model reproduces well the observed light curve with a slight perturbation of a sinusoidal feature, and predicts that a slightly larger period than previously reported, of about 1899 days, could arise due to a cold spot in the disk of more massive component of a close, unequal-mass ($\frac{m_1}{m_2} = 0.1$) black hole binary

system. The light curve resembles the pattern of sinusoid-like shape within a few years, which could be confirmed by future observations. In addition, using our hybrid method for periodicity detection, we show that the periods in the observed (1972 ± 254 days) and modeled (1873 ± 250 days) light curves are within one-sigma, which is also consistent with our physical model prediction and with previous findings. Thus, both the periodic nature and its slight fluctuation of the light curve of PG1302-102 is evident from our physical model and confirmed by the hybrid method for periodicity detection.

Keywords: quasars: individual (PG1302-102), quasars: supermassive black holes — methods: data analysis

1. INTRODUCTION

The hierarchical structure formation model of galaxies suggests supermassive black hole binaries (SMBHB) should be common in the galactic nuclei (see recent analysis [Khan et al. 2016](#); [Kelley et al. 2017](#), and references therein); yet these systems are extremely difficult to identify at sub-parsec separations even in the local Universe ([D’Orazio & Loeb 2017](#)). In the era of multimessenger astrophysics, the importance of the SMBHB at sub-parsec distance surpasses the understanding of evolutionary processes. They are recognized as targets for associating gravitational waves with electromagnetic counterparts ([Bowen et al. 2018](#)). Such a possibility is quite likely, because merging black holes could interact with: a circumbinary accretion disk, remnant gas between the black holes, and a magnetosphere. All these interactions could contribute to electromagnetic counterparts (see [Palenzuela et al. 2010](#), and references therein).

As such compact accreting source can not be resolved spatially, the presence of any periodic signal should be detected indirectly from the SMBHB effects (see e.g. [Popović 2012](#); [Bon et al. 2012, 2016](#); [Li et al. 2016](#)) either on the surrounding accreting gas or precessing jet (see [Charisi et al. 2018](#); [Britzen et al. 2018](#), and references therein). However, these systems exhibit random fluctuations, whose Fourier spectra follow power law with indices larger than zero, so called red noise ([Press 1978](#)), making periodicity more difficult to detect ([Vaughan 2010](#)).

A particularly appealing recent case is the quasar PG1302-102 (Graham et al. 2015). By comparison with other SMBHB candidates, PG1302-102 photometric light curve resembles rather sinusoidal structure. Still, its light curve is not strictly periodic (D’Orazio et al. 2015).

Graham et al. (2015) reports an evidence of a binary system with a ~ 4 yr rest-frame period based on the analysis of data from Catalina Real-Time Transient Survey –CRTS. Additionally, Jun et al. (2015) and D’Orazio & Haiman (2017) reports periodic variability of PG1302-102 in the infrared. Up to now, a new clues to its variability has emerged. Namely, it seems that adding recent observations from All-Sky Automated Survey for Supernovae –ASAS-SN, which are analyzed in details by Liu et al. (2018), shows that the evidence for periodicity decreases, and that further new observations would clarify the significance of the SMBHB model. The first aim of our work is to model the optical light curve with a perturbation in the disk of more massive component in the SMBHB (Popović & Simić 2018) which slightly perturb the sinusoidal signal and to forecast the light curve variability in the next few years. The reason for choosing such approach is that the standard SMBHB model assumes that an accretion disk surrounds at least more massive black hole and that the outcoming variability and structural changes are determined by dynamical characteristics of the disk as well as the interaction of the SMBHB–disks system (Lobanov & Roland 2005). The second aim is to test our newly proposed hybrid method for oscillation detection in the light curves of quasars (which was presented in Kovačević et al. 2018), on both observed and modeled light curves.

The structure of the paper is as follows. We first introduce our physical model in Section 2. We then present briefly the data and hybrid method for periodicity detection in Section 3. The results are described and discussed in Section 4. Summary of our findings concludes our paper in Section 5.

2. THE MODEL: SMBBHS AND PERTURBATION IN THE EMISSION DISK

There are several approaches to model the emission from the SMBHB (see Popović 2012, and references therein). Here we utilize the model described in Simić & Popović (2016). The model is able to include perturbations in one of the component disks (or both of them) which are resulting in either an amplification or attenuation of the flux of the system. The model can be shortly described as following. Adopted geometry of the SMBHB system assumes two supermassive black holes (with

mass of a less massive component m_1 , and more massive component m_2 , i.e. $\mathbf{m}_1 < \mathbf{m}_2$ and $\mathbf{q} = \frac{\mathbf{m}_1}{\mathbf{m}_2}$) which orbit the barycenter of the system, in the plane inclined at an angle θ with respect to the observer. Accretion disks around each black holes are coplanar with the orbital plane.

Both accretion disks are classical geometrically thin optically thick relativistic disk proposed by [Shakura & Sunyaev \(1973\)](#), which are thermalized due to the friction of rotating matter and radiate continuum emission in the UV, optical and IR band. The disk effective temperature (T_{eff}) decreases with the radius R , and is given with the following expression adopted from [Lasota \(2016\)](#):

$$T_{\text{eff}}[K] = 2 \cdot 10^5 \left(\frac{10^8}{m_i} \right)^{1/4} \left(\frac{R_{\text{in}}}{R} \right)^{3/4} \left(1 - \sqrt{\frac{R_{\text{in}}}{R}} \right) \quad (1)$$

where $m_{i,i=1,2}$ is black hole mass and R_{in} is inner radius.

There are several empirical definitions of the radius of an accretion disk ([Krolik & Hawley 2002](#)), and some more for slim accretion disks ([Abramowicz et al. 2010](#)). In our work the inner radius is defined as $R_{\text{in}} \propto 10R_g$, where R_g is the half of the Shwarzschild radius, because it emphasizes the inner most place from which the UV/optical/IR luminosity originates. Moreover, we also consider that the inner radius corresponds to the innermost stable circular orbit (ISCO).

To estimate the outer radius R_{out} in units of light days, we adopt the relation given by [Vicente et al. \(2014\)](#), which is coming from the microlensing observations of quasars:

$$R_{\text{out}[ld]}^i = \frac{1}{2} \cdot r_0 \left(\frac{m_i [\text{M}_\odot]}{10^9} \right)^{2/3}. \quad (2)$$

where $r_0 = 4.5(\pm_{1.6}^{0.7})$, and mass m_i is given in solar masses. The outer radius of the accretion disks around black holes in a compact binary system on a circular orbit, could be tidally truncated (see [Paczynski & Rudak 1980](#); [Papaloizou & Pringle 1977](#); [Roedig et al. 2014](#)). We also consider this scenario, setting the outer radius of the disk of the more massive component to $R_{\text{out-lc}} \sim 0.27q^{-0.3}a$ and of the less massive component to $R_{\text{out-sc}} \sim 0.27q^{0.3}a$, where a is a separation of components, $q = \frac{\mathbf{m}_1}{\mathbf{m}_2}$ is the mass ratio of components, and $\mathbf{m}_1 \leq \mathbf{m}_2$. The ratio of outer radii inferred from Eq. 2 ($\frac{R_{\text{out-lc}}}{R_{\text{out-sc}}} \sim q^{0.67}$) is almost the same as in the case of tidally truncated binary system considered above ($\frac{R_{\text{out-lc}}}{R_{\text{out-sc}}} \sim q^{0.6}$). Thus, Eq. 2 can be adopted for calculating the disk dimensions.

The emission from both disk has a black body distribution and the summarized luminosity $L(\lambda)$ at wavelength λ from all parts of disk with different effective temperature is given with:

$$L(\lambda) \propto \int_{S_{\text{disc}}} \lambda dL(\lambda, T_{\text{eff}}) \quad (3)$$

where S_{disc} is the area of the considered disk.

Due to the loss of energy, black holes in a binary system approach each other over time. Consequently, mutual interaction between one disk and opposite black hole component arises. This interaction can perturb the disk temperature profile, causing the luminosity variation. Also, in compact binary systems (where the distance between black holes is smaller than 0.1 pc), the radial velocities of components can increase to the relativistic values. In that case, the effect of relativistic boosting can have an important influence. Both of those effects are taken into account in our model. Their detailed description is given in [D' Orazio et al. \(2015\)](#); [Simić & Popović \(2016\)](#). Our model will be described in more details in [Popović & Simić \(2018\)](#).

With this dynamical model we are able to reproduce light curves for SMBHB systems with different parameters. As an example we present in [Figure 1](#) brightness variation for the object PG1302-102. In this case we take the time evolution of the proposed binary system for four full orbits, for which we use a grid of 200 computational points, although a higher number can be considered. We test various models to roughly fit the observed PG1302-102 light curve, and find that a model with the following parameters: $m_1 = 10^8 M_\odot$, $m_2 = 10^9 M_\odot$, $R = 0.015$ pc, $\theta = 45^\circ$, $e = 0$, and orbital period $P = 1899$ days, can nearly describe the PG1302-102 light curve in the first period. The light curves during four orbital periods of each component are shown in plot (a) and the resulting (total) light curve in plot (b) in [Figure 1](#). As one can see, there is a phase shift of local extrema of components, due to the opposing radial velocities. This indicates that the relativistic boosting plays a dominant role in such case, and that the mutual interaction is almost negligible. We also see that the variability of one component is higher than the total luminosity variation, especially in the case of a less massive component. The pure dynamical model, cannot explain the part of PG1302-102 light curve beyond

5000 days (see [Liu et al. 2018](#)), therefore we consider that an additional attenuation in the brightness of the SMBHB should be present.

2.1. *Perturbation in an accretion disk*

One purpose of our model is to simulate the long-term variability in SMBHBs. The variability can be caused by the dynamical parameters of the system, as it is shown in Figure 1, but also by the intrinsic variability of one of the components. As often observed in the light curves of single active galactic nuclei (AGN), under long-term monitoring, the flux perturbations are present in the form of outbursts ([Shapovalova et al. 2010](#); [Graham et al. 2017](#)), long-lasting flares as in the case of binary black hole candidates NGC 4151 (see Fig. 2 in [Shapovalova et al. 2008](#)) and E1821+643 ([Shapovalova et al. 2017](#)), or as remarkable low states or minimum states characterized by an exceptionally weak continuum and line fluxes, also seen in the case of binary black hole candidates NGC 4151 ([Shapovalova et al. 2008](#)) and NGC 5548 ([Bentz et al. 2007](#)). The long term variability of some objects has been successfully modeled by the variety of disk perturbations ranging from the precession of an elliptical disk, or a disk with a spiral arm, to bright spots, highly-ionized fast accretion disk's outflows, as well as rotated, sheared, and decayed bright spots (see [Jovanović et al. 2010](#); [Popović et al. 2012](#), and references therein) and cold spots ([Kasliwal et al. 2017](#)).

The perturbations are well localized in the light curve, which possibly reflect the sharp edges of the emission region, and are usually resembling to a Gaussian-like form. If the angular dimension of the emission region is much smaller than the viewing angle, a distant observer could not detect the anisotropy of its radiation. Based on the above reasons, the perturbations in the light curves have been modeled with Gaussian, exponential, and various other functional forms (e.g. [Valtaoja et al. 1999](#); [Kudryavtseva et al. 2011](#); [Angelakis et al. 2015](#)). [Kaulakys & Alaburda \(2009\)](#) and [Kelley et al. \(2011\)](#) proposed models of light curves based on superpositions of exponentially decaying perturbations occurring at random times and with random amplitudes (the latter is also recognized as Gaussian Process Regression). Gaussian-like perturbations could arise from the intrinsic quasar variability, for example the convergence of the Poissonian process once applied to the AGN light curve as reported by [Pecháček et al. \(2008, 2013\)](#) can be understood in the general statistical sense

as convergence to the Gaussian random process (Fageot et al. 2017). Based on previous discussion, there is some evidence that the Gaussian-shaped perturbations are seen in AGN and even in magnetohydrodynamical simulations, though it is not the only type that can emerge.

Usually considered perturbation is in the form of an outburst, which is obtained directly from the magnetohydrodynamic simulation with a hot spot in the disk (Balbus & Hawley 1991; Armitage & Reynolds 1992; Abramowicz et al. 1992; Poutanen & Fabian 1999; Życki 2002; Nayakshin et al. 2004; Dai et al. 2010), as well as with a multicomponent spot settings (Schnittman et al. 2006; Pecháček et al. 2008, 2013; Zamaninasab et al. 2010). It is important to note that, as reported by Valtaoja et al. (1999), the magnetohydrodynamic models can explain the physics underlying the flare appearance and its overall shape but cannot provide its exact functional time dependence as phenomenological models can.

In the case of PG1302-102, the drop in the brightness is seen, resembling the form of an inverted Gaussian-like flare (see Figure 1 in Liu et al. 2018), suggesting the local temporal decrease of the disk temperature. This feature in the light curve could be associated with cold spots (Kasliwal et al. 2017) or even with relatively small, dusty, rapidly-moving clouds partially covering the continuum and broad line region of a quasar (Gaskell & Harrington 2018). Cold spots could be intuitively understood as relatively confined subluminal regions like sunspots (Gould & Miralda-Escudé 1997). The cold clumps could form naturally as a result of thermal instability in the hot gas (Yuan 2003) or condensation of the hot flow (Róžańska & Czerny 2000; Liu et al. 2007; Meyer et al. 2007; Mayer & Pringle 2007; Meyer et al. 2009; Liu et al. 2011).

Thus, the Gaussian profile is taken in our model for simplicity, and we assumed that the appearance of a cold spot causes the flux attenuation in the light curve of PG1302-102. Moreover, if we consider asymmetrical perturbation, i.e Poissonian, it would affect the shape of the modeled inverted hump in the light curve, by producing an asymmetry on the descending slope as two stacked peaks. However, such feature is not supported by the observed data of PG1302-102. The reason for this might be found in differences between gradients of Poissonian slopes and those in the observed inverted hump. Namely, a Poissonian descending slope is much slower than the corresponding slope in the observed

hump in PG1302-102. However, a Gaussian perturbation is symmetric with much faster descending slope, which is in better agreement with the data, and supports our assumption to use Gaussian perturbation.

2.2. Gaussian-like disk perturbation - model

Following the previous section discussion, in our phenomenological model we include the conceptual Gaussian-like perturbation. To model the Gaussian-like perturbation in one component, we propose the temperature perturbation of the disk in more massive black hole (as it is shown in Figure 2, upper panels). It is proposed that the whole body of the disk is perturbed, where the perturbation reaches an absolute extremum value of approximately 1.7%. Applied perturbation changes in time the disk temperature profile ($T_{\text{eff}}^{\text{pert}}(R, t)$) according to the following expression:

$$T_{\text{eff}}^{\text{pert}}(R, t) = T_{\text{eff}}(R) + T_{\text{eff}}(R) \cdot \delta T(t), \quad (4)$$

$$\delta T(t) = P_{\text{int}} \cdot \exp \left[-\frac{(t - t_{\text{pert}})^2}{P_{\text{dur}}^2} \right] \quad (5)$$

where $T_{\text{eff}}(R)$ is the unperturbed disk temperature profile. Note that a multiplication in the time domain is equivalent to a convolution in the frequency domain. The Gaussian kernel is the physical equivalent of the mathematical point. It is not strictly local, like the mathematical point, but semi-local. Over its lifetime, the perturbation produces a coherent temperature perturbation sampled by a window function $\delta T(t)$. The sign of the intensity of the temperature perturbation, P_{int} , determines whether it is a magnification (positive sign) or an attenuation (negative sign). Our numerical tests confirmed that an inverted Gaussian-like temperature perturbation results in the inverted Gaussian-like shape of luminosity curve. The perturbation is applied on the disk temperature profile of the more massive component and then superposed with an emission from the less massive black hole. As we can see in Eq. 5 the perturbation decreases temperature at instant t_{pert} , for amount P_{int} and duration P_{dur} (Figure 2).

The parameters of the perturbation are found when comparing the modeled and observed data, using the condition of minimization of statistical parameters which defines the goodness of the fit.

Here we intentionally model the Gaussian-like perturbation using three free parameters (instead of two) in order to allow more flexibility in the fitting procedure.

In Figure 2, for example two hypothetical perturbations are present: first, that occurs 1800 days after the beginning of the monitoring, with an extremum intensity of $P_{int} = 3.5\%$ of the total disk emission, and duration of 1000 days (upper left panel (a)); the influence on the more massive component light curve (middle left panel (c)) and the SMBHB light curve (bottom left panel (e)) are also presented. Also, we explore a more realistic perturbation at around 5300 days after the first observation, lasting for 330 days and with lower intensity $P_{int} = 1.7\%$. Its shape and the effects are given in Figure 2 (right panels (b) and (d)). As can be seen from the bottom panels, a perturbation in the disk of one of the SMBHB component can significantly deform the periodical shape of the total SMBHB light curve (compare (b) panel in Figure 1 with the bottom panels (e) and (f) in Figure 2).

Summarizing, our SMBHB model provides the following parameters: black hole masses m_1 , m_2 , $m_1 \leq m_2$, their separation a , inclination of their orbital plane θ , eccentricity e which is the same for both black hole orbits, orbital period P , time t_{pert} when an extremum occurs in the disk of m_2 , intensity P_{int} , and the duration at half of the perturbation P_{dur} .

3. DATA AND METHOD

In this study we use the photometric light curve of PG1302-102 collected by LINEAR, CRTS and ASAS-SN surveys that were employed for periodic analysis reported in Liu et al. (2018). A detailed description of the data sets can be found in Liu et al. (2018, and references therein) and will not be repeated here. In order to apply our hybrid method for periodicity detection, we mitigate possible effects of the gaps within the light curve, and we thus pre-process the photometric light curve by modeling with a robust Gaussian Process Regression (GP, machine learning) method as reported in Kovačević et al. (2018). Here we use a GP with a non-stationary kernel to fit data, which is obtained by the standard procedure of summation of quasi-periodic and Ornstein-Uhlenbeck (OU) kernels (Kovačević et al. 2017). The modeled GP light curve is given in Figure 3.

We use the hybrid method reported in Kovačević et al. (2018) to determine the periodicity in PG1302-102 time series. The hybrid method, thanks to combination of two well-developed tech-

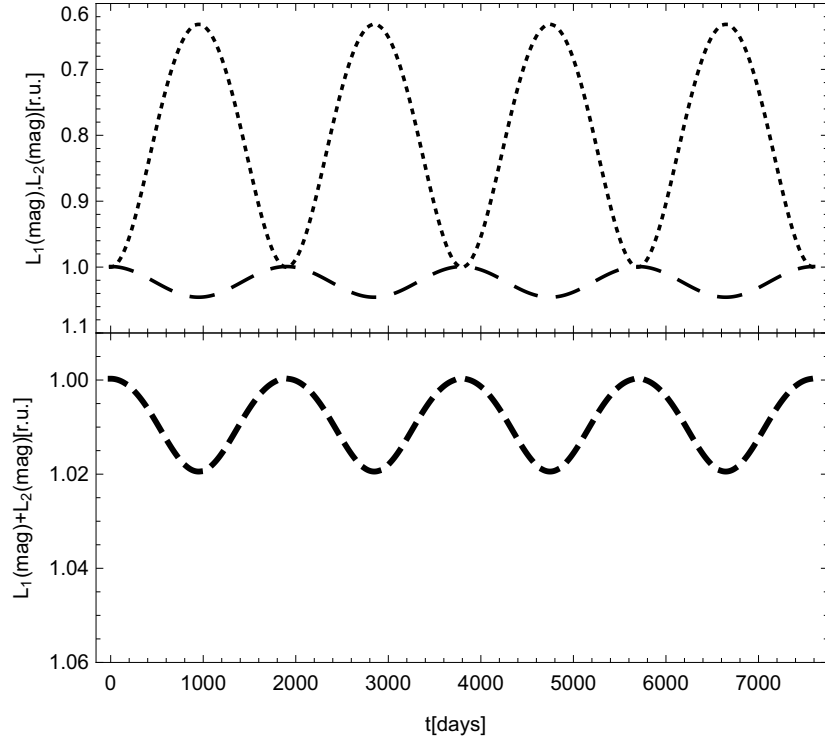


Figure 1. Modeled light curve of the SMBHB system during four orbital periods (see text): (a) Individual light curves (L_1 , L_2) of the corresponding accretion disks of components m_1 (dotted) and m_2 (dashed); (b) The modeled light curve of the total luminosity ($L_1 + L_2$) emitted from the SMBHB. The luminosity is given in relative units on y-axis, and time is given on x-axis in days.

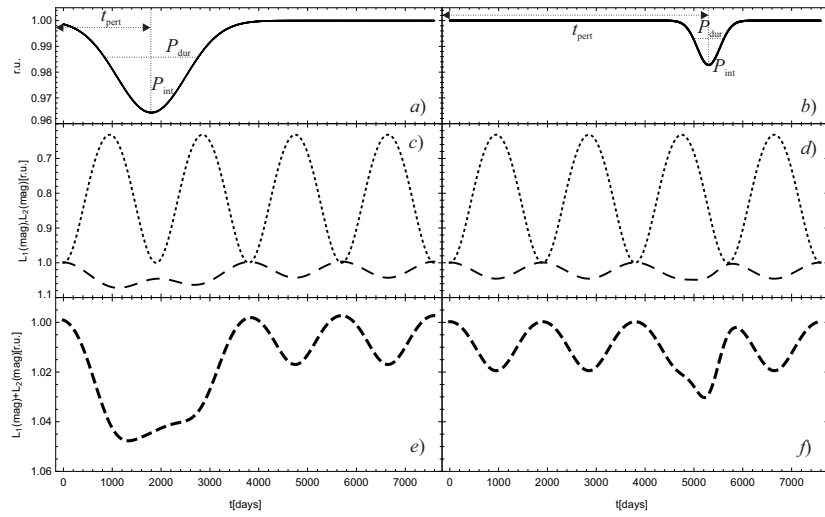


Figure 2. The influence of the different perturbations (the shapes are present in upper panels (a) and (b), see text) on the light curve of more massive component (see middle panels (c) and (d)) and the resulting light curves (shown in bottom panels (e) and (f)).

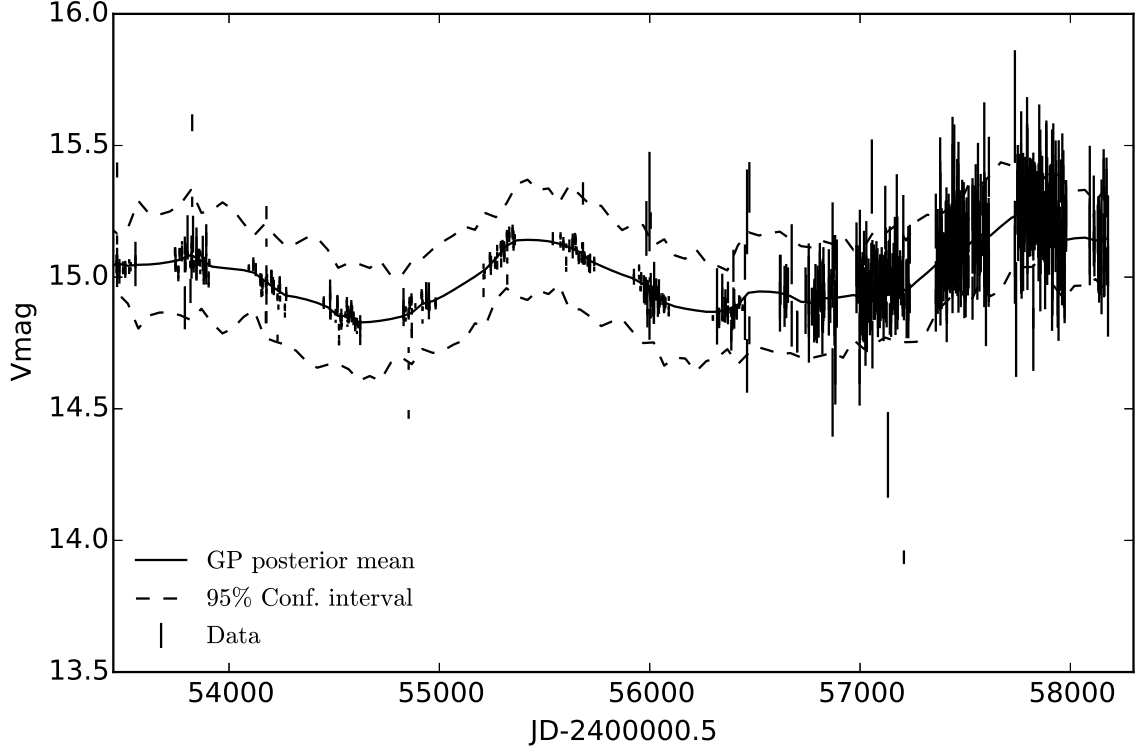


Figure 3. The best fit with a nonstationary GP mean as a solid line with 95% of Confidence Interval between dashed lines. The observed photometric observations are given as vertical error bars.

niques in common use, continuous wavelet transform (CWT) and correlation coefficients, is an easily applicable procedure to the problem of periodicity. Its key advantage over other techniques is that it does not require any assumptions about the stationarity of the data.

The 2D correlation map of periodicities can be calculated in two ways, either using identical or different data sets for an input, as it is a practice in generally similar technique of 2D correlation spectroscopy (Noda 2015). The 2D correlation map of identical data sets deconvolves and determines correlations between periodicities in one light curve. In the case of PG1302-102 we use this approach due to availability of a single light curve. The 2D correlation map involves evaluation of the envelope of CWT of the light curve, after which a nonparametric Spearman's rank correlation for all possible pairs of the values of the envelope is calculated, generating two-dimensional matrix of negative and positive correlations. Note that due to the normalization of correlation coefficients, the correlation coefficient intensity at the main diagonal position is of the order 1, thus influencing the prominence

of correlation clusters which indicates presence of oscillatory patterns. The diagonal feature in the case of identical data sets is more evident, and in the case of different data sets with specific physical dynamics and/or observational characteristics, diagonal can be broken and/or correlation clusters detached. Moreover, in the case of perfect correlation over all periods, the topology of the map would resemble a homogeneous cone, with an apex and an open-end in the lower left and the upper right corner, respectively. Generally, as in the 2D correlation spectroscopy, the noise in the data affect correlation clusters to appear broader and smeared.

After applying the hybrid method on observed light curve, we perform consistency check of the result supported by non linear fitting sinusoid, which has the form of

$$V_{\text{mag}} = A \sin\left(\frac{2\pi t}{P} + \varphi\right) + B, \quad (6)$$

where A is amplitude, P is period, φ is phase and B is offset. The best fit was derived based on the reduced χ^2 .

Since one of the goals of our analysis is to model the perturbation of the periodic signal in the light curve of PG1302-102, it is important to distinct the meaningful signal from the noise, which color is not known *a priori*. A specific test for that noise color must be applied, which we describe in more details and apply on both observed and GP modeled light curve in the following subsection.

3.1. Noise test for the light curve

A red noise process can be interpreted as an autoregressive process of the first order AR(1), with positive correlation at unit lag. A pink noise can be modeled the the differencing parameter $d(=0.5)$ of the Box – Jenkins autoregressive integrated moving average (ARIMA) strategy, taking on it continuous values (Box & Jenkins 1970). Autoregressive fractionally integrated moving average (ARFIMA) modeling improves the Box-Jenkins approach by implementing the differencing parameter d to have non-integer values. This allows ARFIMA to fit any long range memory in time series remarkably (Brockwell & Davis 2002). However, these processes are stationary. If the PG1302-102 light curve is found to be non stationary, then it is different from mentioned noise processes. If the light curve is stationary further statistical procedures must be applied to verify that the light curve

is a noise process. Thus, a stationarity test is first applied on the given light curve. For this purpose we used Kwiatkowski-Phillips-Schmidt-Shin (KPSS) test (Kwiatkowski et al. 1992). The test can be applied on time series with gaps, because simply ignoring gaps or filling them with interpolated values does not alter asymptotic results associated with its statistics. In our analysis the KPSS test, applied to the observed light curve with ignored gaps and to the GP modeled curve, rejects stationary null hypothesis in favor of the non-stationarity alternative at 5% significance level. As the result of the test, the signal is discerned as a subsequences of light curve differing from the noise. Furthermore, we add the white noise to our modeled data in Section 2, since the autocorrelation functions of each cluster of points in the observed light curve correspond to the white noise. It is generated as a random process with a Gaussian distribution, with the mean value of $\mu = 0$ and the absolute value of width σ , which depends on units used. In our computation we normalize flux to 1, so that parameter σ has value around 0.5%, i. e. $\sigma = 0.005$.

In order to investigate the effect of perturbations and added white noise to the modeled light curve, we perform the following numerical experiment. We apply our hybrid method on the hypothetical curve with and without the white noise (see bottom right plot in Figure 2). Our hybrid method gives the period of 1873 ± 250 days in both cases, when white noise is included and excluded. This is in agreement with the period of 1899 days inferred from the model (Section 2). In both cases we could detect the presence of periodicities. However, the uncertainty is large due to large magnitude of perturbation.

4. RESULTS AND DISCUSSION

Using the proposed model from Section 2 we first inferred the observed light curve without white noise (see right plots in Figure 2). Then, the modeled light curve given in Figure 4 is obtained by adding the white noise to the model. As we can see, there is a very good agreement between the observations and model with perturbation for the set of inferred parameters given in Table 1.

The model with perturbation produces orbital period of $P = 1899$ days, and circular orbits. Inferred larger mass and mass ratio is consistent with those obtained in analysis of D' Orazio et al. (2015), while the period estimate is slightly larger for about 10 days then reported in Graham et al. (2015),

Table 1. Inferred parameters of the model of the SMBHB system with Gaussian perturbation in the accretion disk of the more massive component, defined in Section 2. Parameters AIC, BIC, AIC_{np}, BIC_{np}, and AIC_{nc}, BIC_{nc} measure the quality of perturbed, non-perturbed and pure noise model, respectively (see text).

m_1 [$10^8 M_\odot$]	m_2 [$10^8 M_\odot$]	a [pc]	e	t_{pert} [days]	P_{int} [%]	P_{dur} [days]	P [days]	AIC	BIC	AIC _{np}	BIC _{np}	AIC _{nc}	BIC _{nc}
1	10	0.015	0	5300	1.7	330	1899	-4135	-4125	-3793	-3787	-3028	-3025

but still within the error bars. Setting inner radii of both disks to the value of ISCO does not affect the simulated light curve, because the regions close to the black holes radiate photons of much higher energies which do not contribute to the observed band directly. The assumption that the outer radii of the larger and the smaller disks are defined by the tidal truncation (see Section 2), produces negligible variation in the light curve amplitude of approximately several percents.

We used Eq. 2 to calculate the outer radius of both accretion disks, which ratio is around 4, that is very close to the value of 4.6 in the case of tidally truncated binary system, taking into account $q = 0.1$. The difference between these two ratios reflects difference in the luminosity of several percents, additionally, we considered only the perturbation in the more massive component.

We compute the AIC (Akaike Information Criterion) and BIC (Bayesian Information Criterion) parameters which define criteria for model selection and effectiveness (Table 1). In the computation, our model produce simulated light curve for the same time points as given in the observed light curve. Also, in order to have more realistic values of AIC and BIC parameters, model points are computed at the same moment when data points are recorded. Small variations for AIC and BIC values are possible since stochastic nature of included white noise. Note that AIC and BIC of our models differ significantly from those obtained by Liu et al. (2018). This could be due to different normalization of data as well as due to different models. Liu et al. (2018) model is a rational function of short-timescale variance and characteristic time scale (see their equation 4). We calculated the log-likelihood function (L) of the data y_n given the parameters θ as follows

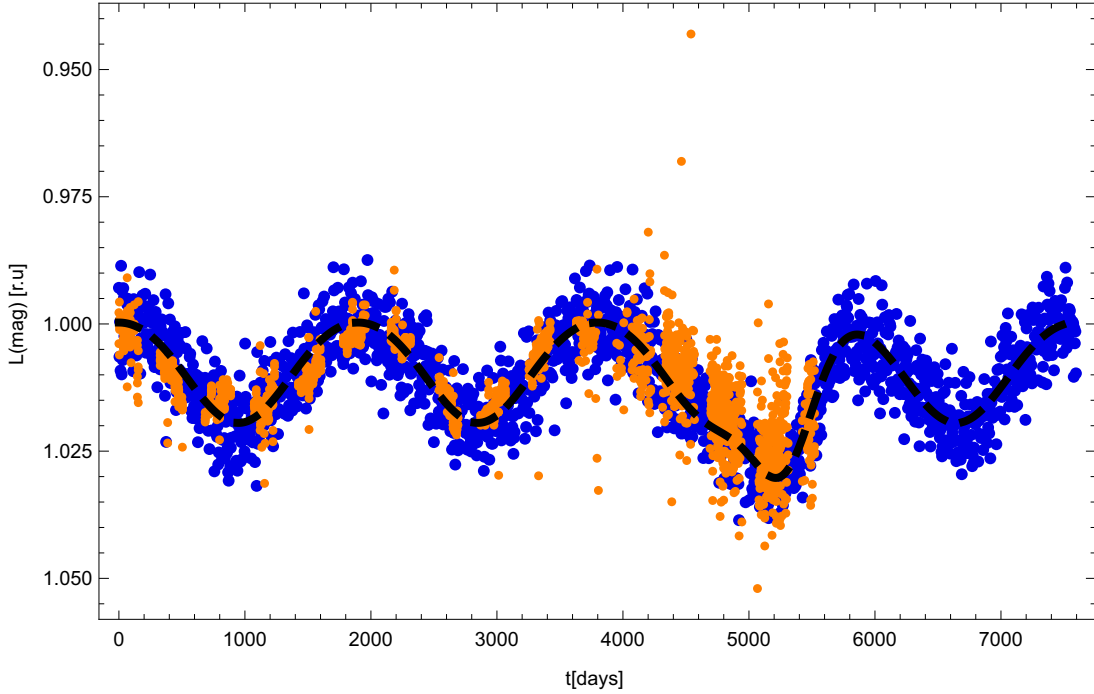


Figure 4. Observed (orange points) and modeled light curve (blue points). Dashed black line represents the modeled curve without white noise. Time is given on x-axis in days, whereas the flux (note that the observed light curve is previously expressed in magnitudes) in relative units is given on y-axis.

$$\ln L = -\frac{1}{2}r^T K^{-1}r - \frac{1}{2}\ln|K| - \frac{N}{2}\ln 2\pi \quad (7)$$

where r is the residual vector between the mean flux predicted in a model and the observed flux at each observation time t_i . Here $K = \sigma_{ij}^2 \delta_{ij}$, $\delta_{ij} = 1, i = j$ and $\delta_{ij} = 0, i \neq j$, is the diagonal covariance matrix where σ_{ij}^2 is the variance. The fact that K is diagonal is the result of our earlier evidence that the data are uncorrelated. The variances are obtained as second derivatives of the likelihood function with respect to the model parameters fitted to the data (i.e. as diagonal elements of the Fisher information matrix). Note that due to different modeling approach, [Liu et al. \(2018\)](#) applied their method only to the binned light curve, which consisted of 19 and 35 barycentric points for LINEAR+CRTS and LINEAR+CRTS+ASASSN data set respectively, assuming that these barycentric points are correlated as damped random walk. The same assumption of correlation between data points was used in [D' Orazio et al. \(2015\)](#) but the data set consisted of about 250

points. This implies that the covariance matrices $K = \sigma_i \delta_{ij} + k(t_i, t_j)$ had non diagonal elements $k(t_i, t_j)$ arising from the assumed damped random walk in these studies.

We note that D’ Orazio et al. (2015) and Liu et al. (2018) analysis did not use Fisher Information matrix as an estimate for their covariance matrices. Instead, former study used log likelihood covariance matrix with added variances in the photometric measurement on the diagonal, and Liu et al (2018) had the Gaussian noise added on the diagonal which could explain AIC differences about 10 in their calculations.

Thus, the major difference between our AIC, BIC and those found in the recent papers most likely lies in the form of covariance matrix constituting the Gaussian likelihood function as well as in the number of used data which affect the dimension of the matrix and later the process of maximization. Our approach is distinct from previous ones in the fact that complete data set of 1700 points which have white noise characteristic is modeled without binning.

Besides general differences in covariance matrix, note that the data of D’ Orazio et al. (2015) does not show attenuation, and that in Liu et al. (2018) study perturbation was not included in their model and due to the binning of the light curve the hump in the light curve was covered by 15 barycentric points which slightly changed the geometry of the hump. The number of points in the hump is about 873 which is almost half of all available data implying that large portion of information lies in the hump too. Our model shows a large difference between the pure noise and perturbed model confirming the importance of information confined in the hump of PG1302-102 light curve.

Moreover, the differences between information criteria of the composite sinusoid-noise and the pure noise model were close to 10 in previous studies. A model with AIC difference strictly larger than 10 units of the best model, which indicates that the model is less favorable, will have no support, and can be omitted from further consideration (Burnham & Anderson 2002). However, models with differences up to 10 are usually considered as no superior to some other models in a set of considered models. In this case model averaging (combining) gives a relatively more stabilized inference (Burnham & Anderson 2002). From this point of view the previous analysis suggests a model combination.

We can see that our model as a composite, consists of three parts: dynamical (sinusoidal), perturbation, and noise part, and demonstrates that light curve is best described with combined model due to large AIC (BIC) difference with respect to the pure noise model, which is in agreement with findings of previous studies. Thus, for the first time, we confirmed that it is possible to model a complete data set of PG1302-102 without any binning, and extract a valuable information of a periodic signal and perturbation.

As for the absolute magnitude of our AIC and BIC, we will note that in the maximum Gaussian log-likelihood solution the weights vector is identical to the least squares solution, which means that the better the independent variables of the model are in predicting the dependent variable, the more negative the AIC becomes. In ideal case it would approach negative infinity. As for the comparison of models, in the case of two models (as it is in our analysis) the statistical rule is to compare only their AIC values (not absolute value), thus model with lower AIC would be the preferred one. Here both AIC and BIC are the smallest for the model with perturbation included. In the case of more than two models the difference between i -th model AIC and minimum AIC among all models is used. It is not possible to use this set of models approach to compare our AIC with those in [Liu et al. \(2018\)](#) analysis due to different Gaussian-likelihood formulation and possible different normalization of data.

Next, we apply our hybrid method to the modeled (Figure 4) and preprocessed observed light curve (Figure 3), for which we tested that it is not the noise process (subsection 3.1).

As can be seen in Figure 5, both curves have almost similar 2D correlation maps. The topology of our 2D correlation map is fragmented and attached correlation clusters are visible. There are two important regions of periods, the largest about 4000 days on both maps and smaller clusters at 1873 ± 250 and 1972 ± 254 days, for modeled and preprocessed observed curve, respectively. Their correlation coefficients are 0.99 with a significance of $p < 0.00001$. The period of ~ 4000 days can be neglected since it corresponds to the whole observing period. It is clear that our method has recovered the period of the modeled light curve successfully. The noise is present especially in the

Table 2. Best fitting parameters and their standard deviations of the sinusoid fitted to the detrended observed data, defined by Eq. 6 in Section 3. The parameters χ^2_{red} is reduced χ^2 value of the fit.

A	P [days]	φ [radian]	B	χ^2_{red}
0.123 \pm 0.003	1950 \pm 150	4.74 \pm 0.84	-0.018 \pm 0.003	1.09

hump of PG1302-102 light curve, which effect is evident on the appearance of the correlation cluster associated with this period.

Also, the hybrid method indicates that the periodicity of the observed light curve is very close to the one found in the modeled one. Interestingly, our hybrid method gives almost identical period for the modeled light curve without white noise.

As a further verification we fit a sinusoid to the detrended (mean value is subtracted) observed light curve, which was selected based on reduced χ^2 by being closest to 1. The obtained best fitting parameters with their standard deviations are given in Table 2.

Figure 6 shows sinusoidal model (see Eq. 6 and Table 2) nicely describing the peaks and troughs of the original data, with reduced χ^2 value of 1.09.

The SMBHB model applied to the optical curve of PG1302-102 explains the variability of the optical flux and its perturbation leading to slight changes in detected orbital period of the system. The model recreates physical conditions in the accretion disk of a more massive black hole causing attenuation and the dynamic properties of the system. On the other hand, the model cannot *a priori* predict the repetition of the perturbation, but we can provide some general statistical estimates following the prescription given in Schnittman (2005). If we assume that the characteristic lifetime of the perturbation is about 400 days, as it is the duration of the inverted Gaussian-like perturbation inferred from our model, then the number of such events which could be expected with the life time between 400 and 450 days over the next 2000 days is about 1.7. Based on this pure statistical view, there is a chance to detect a similar event within next few years.

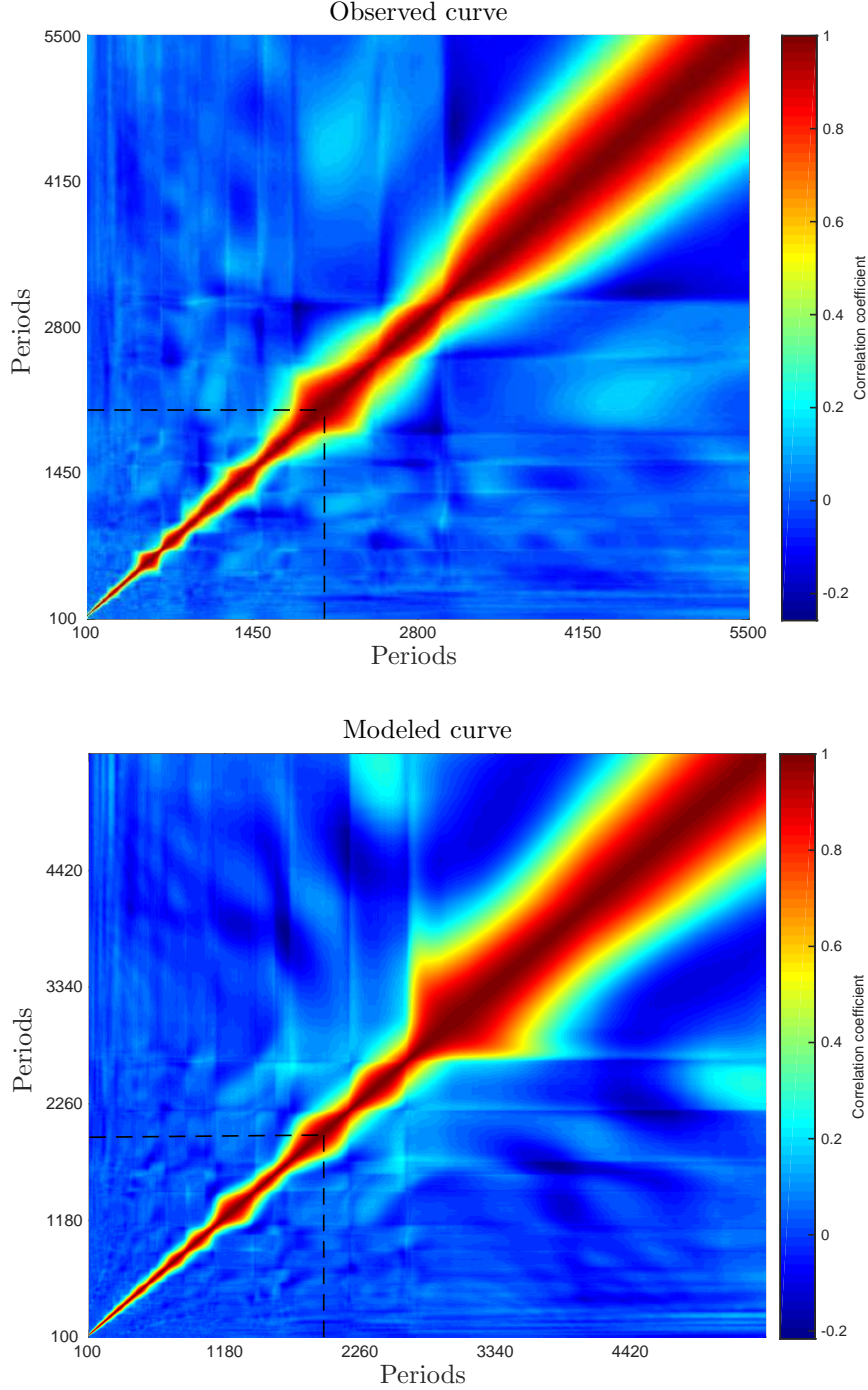


Figure 5. The 2D correlation map of all oscillatory patterns within the total observing time range 100 – 5500 days, for preprocessed observed light curve (top) and modeled light curve (bottom). Both axes represent periods (in days) in the curve. Diagonal correlation clusters means that oscillations are caused by physical processes within PG1302-102. Values of correlation coefficients are given on colorbar. The clusters of high correlation are marked in red with significance $p < 0.00001$. Dashed line marks detected period.

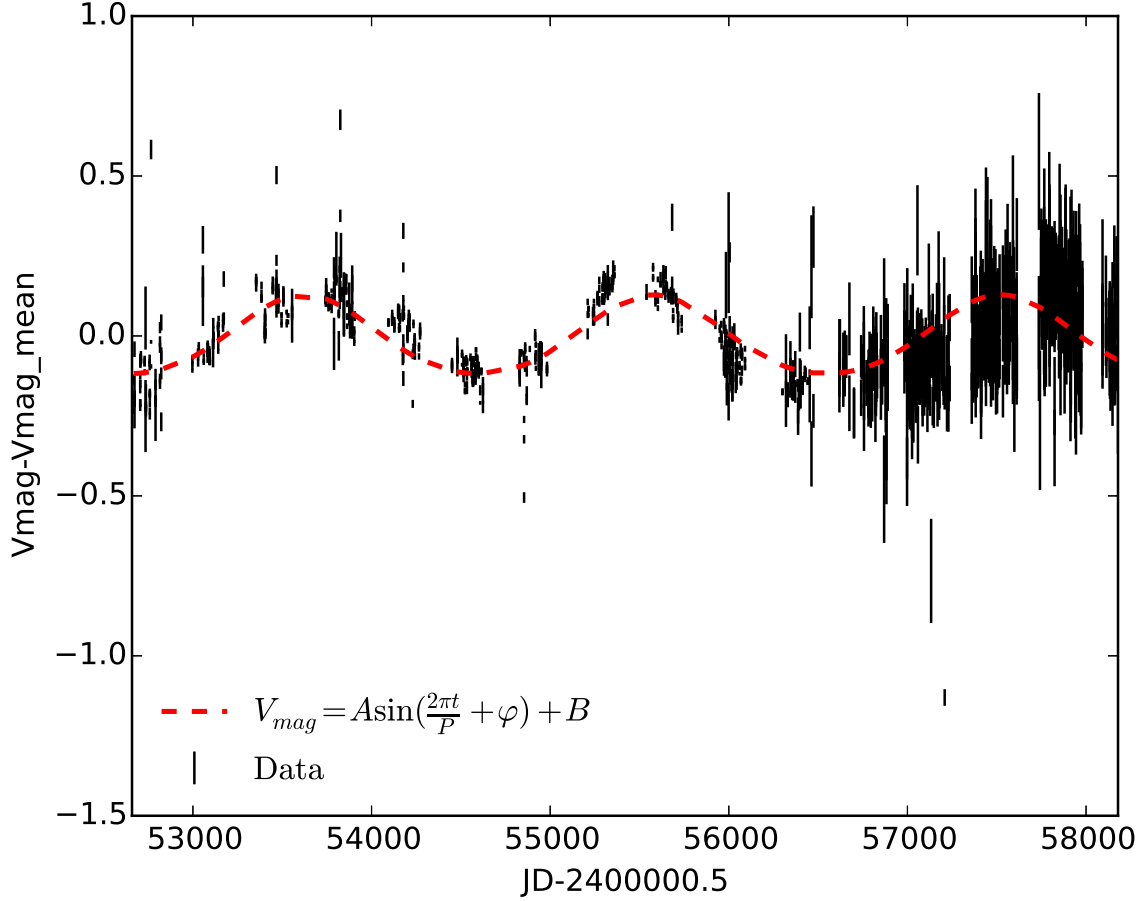


Figure 6. Best fitting of sinusoid model to the detrended (mean value is subtracted) observed light curve. Photometric magnitudes are represented by error bars whereas model with dashed, red line. The best fitting parameters are given in Table 2.

In our analysis we consider one time event, because the data did not show any similar feature up to now. The recurrence of perturbations is well analyzed by the magnetohydrodynamic simulations directly producing the hot spots in the accretion flow and implying that these phenomena could be either periodic (and destroyed by differential rotation) or aperiodic (Fukue 2003). Based on this, something similar could be expected for cold spots. Thus, if the perturbation in PG1302-102 light curve is periodic, there is also a possibility that its next amplitude would appear smaller due to differential rotation which can gradually destroy it.

Moreover, Valtaoja et al. (2000) pointed to a possibility that at certain intervals the less massive black hole crosses the accretion disk of the more massive black hole, and the effect of shadowing

the certain parcel of the disk could be expected (Abramowicz & Fragile 2013). This means that the peak from such event should be broader in time, because the passing takes longer than the crossing. Such dynamical relation (and its signal) is likely to be periodic, but with periods of the order of decades to centuries. Thus, we are likely to detect separate events and anticipate them as isolated flares (Bogdanović et al. 2008). Moreover, linking the circumbinary disk to the mini-disks and the gas density at the inner edge of the circumbinary disk, a lump has been observed in the recent magnetohydrodynamic simulations of binary black hole systems (MacFadyen & Milosavljević 2008; Shi et al. 2012; D’Orazio et al. 2013; Farris et al. 2014; Shi & Krolik 2015; D’Orazio et al. 2016; Tang et al. 2017, 2018). A generic result of these simulations is a low-density cavity created by the binary torque, but gas can still leak into the cavity through non-axisymmetric streams, implying lower temperature in such region. Recently, Tanaka (2013) proposed that periodic streams into the cavity may activate more noticeable variability than previously thought.

However, the first general relativistic magnetohydrodynamic simulation (Bowen et al. 2018), assuming that the binary separation is relativistic, revealed even more dramatic picture. Namely, the response of the accretion disks around black holes to the circumbinary disk in the binary system may introduce distinctive time-dependent features in the binary’s electromagnetic emission.

Instead of a single perturbation, multiple perturbations can appear in the disk, which may lead to the superposition of their individual luminosities into a complex signal, and a periodicity analysis is required. However, the structure of the data in the inverted hump of PG1302-102 is not favorable of this scenario, and the periodicity analysis could not disentangle superimposed signals if any present.

Perturbations were recorded in the light curves of some well studied objects as we mentioned in Subsection 2.1. The most comprehensive study to date, specifically focused on a systematic search for major flares in AGN, is by Graham et al. (2017). They presented remarkable results of the CRTS, identifying 51 events from the sample of more than 900000 quasars, typically lasting 900 days. The inverted hump of PG1302-102 is within this time range, however the physical explanations suggested by Graham et al. (2017) such as single point single lens model, supernova or tidal distribution events, are not applicable in the case of observed PG1302-102 inverted hump.

As we discussed, there is some chance that the cold spot event occurs in the future, which could affect the light curve over certain range of time. This event could be superimposed on main sinusoidal signal of PG1302-102 binary candidate, but this main periodic signal could be still extracted as it is shown by our hybrid method.

As we have already mentioned, there are physical possibilities for flaring appearances ranging from density irregularities within the disk, up to dynamical reasons as it is a companion black hole producing shadow at the disk after entering the disk.

Moreover, companion black hole radiation could be also important (Pietilä 1998). This object could experience increased accretion when it crosses the accretion disk, passes the pericenter, and crosses in front of the jet. All these instances cause increased flux via temporary accretion disk and jet formation in the companion. There is also another scenario related to circumbinary disk (which may be a condition for some binaries to overcome the *final parsec* barrier), having a large cavity (see Tanaka 2012, and references therein). After passing through pericenter near one of the SMBHs, the stream could self-intersect and produce a shock. This material would circularize into a hot, optically thick annulus and viscously spread. The gas will begin to accrete in a slim-disk form (Strubbe & Quataert 2009) before it can cool radiatively, producing flares in optical, UV and X-domain at the rhythm of years to centuries. However, there could be a significant loss of photons if the rays need to pass through much material such as fast moving clouds, or being attenuated by the supermassive black hole silhouette. Sundelius et al. (1997) showed, in the case of multiple black holes, that the process underlying the leading perturbation in the vicinity of the multiple black holes may not have a strictly periodic character. Bearing this in mind, the signal of such flare could have quasi-periodic nature.

The orbiting hot or cold-spot model would be a natural explanation for the observed light curves with flares and associated changes. However, the long term light curves are also well described by a pure red noise, indicating statistical fluctuations in the accretion flow underlying the observed variability. As pointed in Graham et al. (2017) spectroscopic and multiwavelength observations could settle the debate. For example, data from the Large Synoptic Survey Telescope (LSST) will allow

more precise extraction of periodic signal from the light curve which can reveal additional perturbation more precisely. Even now, a simple test of extracting the sinusoidal signal model from the present light curve of PG1302-102 showed that the remainder of series fluctuates between -0.3 and 0.3 mag after MJD 56500. The shape of this feature is coherent and resembles the gradient of the inverted hump seen in the light curve. Other parts of the remainder fluctuate with magnitudes ten times or more smaller, and are negligible in comparison to the main fluctuation. Upcoming large surveys will determine distribution of physical characteristics of flares and their periodic variation which will also help to test the hot spot and red noise models of light curves on larger sample of objects.

5. CONCLUSION

We develop one possible physical model which could explain the variability of the optical flux and a slight perturbation of sinusoidal feature of the optical light curve of PG1302-102 reported in [Liu et al. \(2018\)](#). The dynamical properties of PG1302-102 are described by the model of the orbital motion in the SMBHB system and the attenuation due to cold spot in the accretion disk around the more massive black hole. The model recovered orbital period of 1899 days. Second, the 2D correlation maps of oscillatory patterns in the observed and modeled light curve are determined with of our hybrid method for periodicity detection. The inferred periods are 1972 ± 254 and 1873 ± 250 days in the observed and modeled light curves, respectively, which are slightly perturbed values in comparison to the [Graham et al. \(2015\)](#) and close to the period predicted by our physical model. Our model suggests the perturbation within the disk of the more massive component, in the form of a cold spot, as an explanation for the perturbed sinusoidal characteristic of the curve, which also slightly deformed the detected period. Moreover, our model gives the light curve a chance of resembling a sinusoidal variability within a few thousand days. Thus, future monitoring of this object is important, and should bring more light into dynamics of the object.

The authors thank to Suvi Gezari and Tingting Liu for providing the complete data set. This work is supported by the project (176001) *Astrophysical Spectroscopy of Extragalactic Objects of*

Ministry of Education, Science and Technological Development of Serbia. The authors would like to express gratitude to an anonymous Reviewer for comments and suggestions which greatly improved the quality of the manuscript.

REFERENCES

- Abramowicz M. A., Lanza A., Spiegel E. A., Szuszkiewicz E., 1992, *Nat*, 356, 41
- Abramowicz, M. A., Jaroszyński, M., Kato, S., Lasota, J.-P, Różańska, A., Sadowski, A., 2010, *A& A*, 521, A15
- Abramowicz, M. A., Fragile, P. C., 2013, *Living Reviews in Relativity*, 16, id. 1
- Angelakis, E.; Fuhrmann, L.; Marchili, N.; Foschini, L.; Myserlis, I.; Karamanavis, V.; Komossa, S.; Blinov, D.; Krichbaum, T.P.; Sievers, A.; et al., 2015, *A & A*, 2015, 575, A55
- Armitage P. J., Reynolds C. S., 2003, *MNRAS*, 341, 1041
- Balbus S. A., Hawley J. F., 1991, *ApJ*, 376, 214
- Bentz, M. C., Denney, K. D., Cackett, E. M., Dietrich, M., 2007, *ApJ*, 662, 205
- Bon, E., Jovanović, P., Marziani, P., Shapovalova, A. I., Bon, N., Borka Jovanović, V. et al. 2012, *ApJ*, 759, 2, id.118
- Bon, E., Zucker, S., Netzer, H. et al. 2016, *ApJS*, 225, 29
- Bogdanović, T., Smith, B. D., Sigurdsson, S., Eracleous, M., 2008, *ApJS*, 174, 455
- Box, G. E. P., Jenkins, G. M. 1970, *Time Series Analysis, Forecasting and Control*, San Francisco Holden Day
- Bowen, D. B., Mewes, V., Campanelli, M., Noble, S. C., Krolik, J. H., Zilhão, M. 2018, *ApJL*, 853, id. L17
- Britzen, S., Fendt, C., Witzel, G., Qian, S.-J., Pashchenko, I. N. et al. 2018, accepted to *MNRAS*
- Broderick A. E., Loeb A., 2006, *MNRAS*, 367, 905
- Brockwell, P. J., Davis, R. A. 2002, *Introduction to Time Series and Forecasting*. New York: Springer.
- Burnham, K.P., Anderson, D. R., 2002, *Model Selection and Multi-Model Inference A Practical Information-Theoretic Approach*, Springer-Verlag, New York
- Charisi, M., Haiman, Z., Schiminovich, D., D’Orazio, D. J. 2018, *MNRAS*, 476, 4617
- Dai L., Fuerst S. V., Blandford R., 2010, *MNRAS*, 402, 1614
- D’Orazio, D. J., Haiman, Z., MacFadyen, A. 2013, *MNRAS*, 436, 2997
- D’Orazio, D. J., Haiman, Z., Schiminovich, D. 2015, *Nature*, 525, 351
- D’Orazio, D. J., Haiman, Z., Duffell, P., MacFadyen, A., Farris, B. 2016, *MNRAS*, 459, 2379

- D' Orazio D. J., Haiman Z. 2017, MNRAS, 470, 1198
- D' Orazio, D. J., Loeb, A. 2017, sent to ApJ, (arXiv:1712.02362)
- Dovčiak, M., Karas, V., Yaqoob, T. 2004, ApJS 153, 205
- Fageot, J., Uhlmann, V., Unser, M., 2017 Gaussian and Sparse Processes are Limits of Generalized Poisson Processes, submitted to Applied and Computational Harmonic Analysis, arXiv preprint, 1702.05003
- Farris, B. D., Duffell, P., MacFadyen, A. I., Haiman, Z., 2014, ApJ, 783, 134
- Fukue, J., 2003, PASJ, 55, 1121
- Gaskell, C. M., Harrington, P. Z., 2018, MNRAS, 478, 1660
- Graham, M. J., Djorgovski, S. G., Stern, D., Glikman, E., Drake, A. J. et al. 2015, Nature, 518, 74
- Graham, M. J., Djorgovski, S. G., Drake, A. J., Stern, D. et al. 2017, MNRAS, 470, 4112
- Gould, A., Miralda-Escudé, J., 1997, ApJ, 483, L13
- Jovanović, P., Popović, L. Č., Stalevski, M., Shapovalova, A. I., 2010, ApJ, 718, 168
- Jun, H. D., Stern, D., Graham, M. J., Djorgovski, S. G., Mainzer, A., Cutri, R., M., Drake, A. J., Mahabal, A. A. 2015, ApJL, 814, L12
- Karas V., Bao G. 1992, A& A, 257, 531
- Karas V., 1999, PASJ, 51, 317
- Kasliwal, V. P., Vogeley, M. S., Richards, G. T., 2017, MNRAS, 470, 3027
- Kaulakys, B., Alaburda, M., 2009, Journal of Statistical Mechanics: Theory and Experiment, 02, 02051
- Kelly, B. C., Sobolewska, M., Siemiginowska, A., 2011, ApJ, 730, 52
- Kelley, L. Z., Blecha, L., Hernquist, L. 2017, MNRAS, 464, 3131
- Khan, F. M., Fiacconi, D., Mayer, L., Berczik, P., Just, A. 2016, ApJ, 828, 73
- Kovačević, A., Popović, L. Č., Shapovalova, A. I., Ilić, D. 2017, Ap& SS, 362, id. 31
- Kovačević, A. B., Pérez-Hernández, E., Popović, L. Č., Shapovalova, A. I., Kollatschny, W., Ilić, D. 2018, MNRAS, 475, 2051
- Krolik, J. H., Hawley, J. F., 2002, ApJ, 573, 754
- Kudryavtseva, N.A., Gabuzda, D.C., Aller, M. F., Aller, H.D., 2011, MNRAS, 415, 1631
- Kwiatkowski, D., Phillips, P. C. B., Schmidt, P., Shin, Y. 1992, Journal of Econometrics, 54, 159
- Lasota, J.-P., 2016, Astrophysics of Black Holes: From Fundamental Aspects to Latest Developments, Editor: Bambi, C., Chapter: Black Hole Accretion Discs, Springer Berlin Heidelberg, 1-60
- Liu, B. F., Taam, R. E., Meyer-Hofmeister, E., Meyer, F., 2007, ApJ, 671, 695
- Liu, B. F., Done, C., Taam, R. E., 2011, ApJ, 726, 10
- Li, Y.-R., Wang, J.-M., Ho, L. C., Lu, K.-X., Qiu, J., Du, P., Hu, C., Huang, Y.-K., Zhang, Z.-X., Wang, K., Bai, J.-M. 2016, ApJ, 822, 4

- Liu, T., Gezari, S., Coleman Miller, M. 2018, *ApJL*, 859, id. L12
- Lobanov, A. P., Roland, J. 2005, *A&A*, 431, 831
- MacFadyen, A. I., Milosavljević, M., 2008, *ApJ*, 672, 83
- Mayer M., Pringle J. E. 2007, *MNRAS*, 376, 435
- Meyer, F., Liu, B. F., Meyer-Hofmeister, E., 2007, *A&A*, 463, 1
- Meyer-Hofmeister E., Liu B. F., Meyer F., 2009, *A&A*, 508, 329
- Nayakshin S., Cuadra J., Sunyaev R., 2004, *A&A*, 413, 173
- Noda, I., 2015, *Biomedical Spectroscopy and Imaging*, 4, 109
- Paczynski, B., Rudak, B., 1980, *AcA*, 30, 237
- Palenzuela, C., Lehner, L., Liebling, S. L. 2010, *Science*, 329, 927
- Papaloizou, J., Pringle, J. E., 1977, *MNRAS*, 181, 441
- Pietilä, H., 1998, *ApJ*, 508, 669
- Pecháček T., Karas V., Czerny B. 2008, *A&A*, 487, 815
- Pecháček, T., Goosmann, R. W., Karas, V., Czerny, B., Dovčiak, M.. 2013, *A & A*, 556, id. A77
- Popović, L. Č. 2012, *NewAR*, 56, 2-3, 74
- Popović, L. Č. Jovanović, P., Stalevski, M., Anton, S., Andrei, A. H., Kovačević, J., Baes, M., 2012, *A & A*, 538, id. A107
- Popović, L. Č., & Simić, S. 2018, in preparation
- Poutanen J., Fabian A. C., 1999, *MNRAS*, 306, L31
- Press, W. H. 1978, *Comments on Modern Physics*, Part C - Comments on Astrophysics, 7, 103
- Roedig, C., Krolik, J. H., Coleman, M. M., 2014, *ApJ*, 785, 115
- Róžańska, A., Czerny, B., 2000, *A & A*, 360, 1170
- Schnittman, J. D., 2005, *ApJ*, 621, 940
- Schnittman J. D., Krolik J. H., Hawley J. F. 2006, *ApJ*, 651, 1031
- Shahbaz, T. 1999, *JA&A*, 20, 197
- Shakura, N.I., & Sunyaev, R. A. 1973, *A&A*, 24, 337
- Shapovalova, A. I., Popović, L. Č., Collin, S., Burenkov, A. N., Chavushyan, V. H. et al. 2008, *A & A*, 486, 99
- Shapovalova, A. I., Popović, L. Č., Burenkov, A. N., Chavushyan, V. H., Ilić, D. et al. 2010, *A & A*, 517, id. A42
- Shapovalova, A. I., Popović, L. Č., Chavushyan, V. H., Afanasiev, V. L., Ilić, D. et al., 2017, *MNRAS*, 466, 4759
- Shi, J.-M., Krolik, J. H., Lubow, S. H., Hawley, J. F. 2012, *ApJ*, 749, 118
- Shi, J. M., Krolik, J. H., 2015, *ApJ*, 807, id. 1
- Simić, S., & Popović, L. Č. 2016, *ApJS*, 361, 59
- Stella, L., Vietri, M. 1999, *Phys. Rev. Lett.*, 82, 17
- Strubbe, L. E., Quataert, E., 2009, *MNRAS*, 400, 2070
- Sundelius, B., Wahde, M., Lehto, H. J., Valtonen, M. J., 1997, *ApJ*, 484, 1, 180

- Tanaka, T., 2012, Tidal Disruption Events and AGN Outbursts, Edited by Saxton, R., Komossa, S., EPJ Web of Conferences, 39, id.06008
- Tanaka, T. L., 2013, MNRAS, 434, 2275
- Tang, Y., MacFadyen, A., Haiman, Z., 2017, MNRAS, 469, 4258
- Tang, Y., Haiman, Z., MacFadyen, A., 2018, MNRAS, 476, 2249
- Valtaoja, E., Lähteenmäki, A., Teräsranta, H., Lainela, M., 1999, ApJS, 120, 95
- Valtaoja, E., Teräsranta, H., Tornikoski, et al., 2000, ApJ, 531, 744
- Vaughan, S. 2010, MNRAS, 402, 307
- Vicente, J. J., Mediavilla, E., Kochanek, C. S., Munoz, J. A., Motta, V., Falco, E, & Mosquera, A. M. 2014, ApJ, 783, 47
- Yuan, F., 2003, ApJ, 594, L99
- Zamaninasab M., Witzel G., Eckart A., 2010, A&A, 510, A3
- Zamaninasab, M., Eckart, A., Dovčiak, M., Karas, V. 2011, MNRAS, 413, 322
- Życki, P. T. 2002, MNRAS, 333, 800